Journal of Power Sources 196 (2011) 8843–8849

Contents lists available at ScienceDirect

Journal of Power Sources

journal homepage: www.elsevier.com/locate/jpowsour

Pulsed laser deposition of manganese oxide thin films for supercapacitor applications

Dongfang Yang*

Industrial Materials Institute, National Research Council Canada, 800 Collip Circle, London, ON, N6G 4X8,Canada

ARTICLE INFO

Article history:
Received 10 May 2011
Received in revised form 9 June 2011
Accepted 10 June 2011
Available online 17 June 2011

Keywords:
Electrochemical capacitor
Supercapacitor
Ultracapacitor
Pulsed laser deposition
Manganese oxides
Thin films

ABSTRACT

Thin films of manganese oxides have been grown by the pulsed laser deposition (PLD) process on silicon wafer and stainless steel substrates at different substrate temperatures and oxygen gas pressures. By proper selection of processing parameters such as temperature and oxygen pressure during the PLD process, pure crystalline phases of Mn_2O_3, Mn_3O_4 as well as amorphous phase of MnO_x were successfully fabricated as identified by X-ray diffraction. The pseudo-capacitance behaviours of these different phases of manganese oxides have also been evaluated by the electrochemical cyclic voltammetry measured in 0.1 M Na_2SO_4 aqueous electrolyte at different scan rates. Their specific current and capacitance determined by electrochemical measurements were compared and the results show that crystalline Mn_2O_3 phase has the highest specific current and capacitance, while the values for crystalline Mn_3O_4 films are the lowest. The specific current and capacitance values of the amorphous MnO_x films are lower than Mn_2O_3 but higher than Mn_3O_4. The specific capacitance of Mn_2O_3 films of 120 nm thick reaches 210 F g^{-1} at 1 mV s^{-1} scan rate with excellent stability and cyclic durability. This work has demonstrated that PLD is a very promising technique for screening high performance active materials for supercapacitor applications due to its excellent flexibility and capability of easily controlling chemical composition, microstructures and phases of materials.

Crown Copyright © 2011 Published by Elsevier B.V. All rights reserved.

1. Introduction

Supercapacitors store energy using either ion adsorption (electrochemical double layer capacitors) or fast surface redox reactions (pseudo-capacitors). Electrochemical double layer capacitors use high surface area activated carbon as the active electrode materials, while metal oxides, such as RuO_2, Fe_3O_4 or MnO_2, as well as electronically conducting polymers, are used as the active electrode materials for the pseudo-capacitors [1]. The specific pseudo-capacitance of metal oxides typically exceeds double layer capacitance of carbon materials due to involving the Faraday charge transfer reactions. Among all the metal oxides, specific pseudo-capacitance of RuO_2 is one of the highest and its pseudo-capacitive behaviours have been most widely studied. However, RuO_2 is expensive which limits its wide scale applications. Manganese oxide is regarding as the most promising candidate material among the less expensive metal oxides to replace RuO_2 for pseudo-capacitors. It is relatively low cost, low toxicity, and environmental friendly. The charge storage mechanism of manganese oxide based on surface adsorption of electrolyte cations as well as proton incorporation which accompanies the oxidation/reduction of Mn ions is in according with the following reaction:

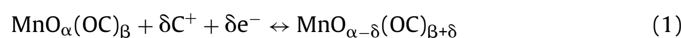

$$MnO_{\alpha}(OC)_{\beta} + \delta C^{+} + \delta e^{-} \leftrightarrow MnO_{\alpha-\delta}(OC)_{\beta+\delta} \quad (1)$$

where C^+ denotes the protons (H^+) and alkali metal cations (Li^+, Na^+, K^+) in the electrolyte, and $MnO_{\alpha}(OC)_{\beta}$ and $MnO_{\alpha-\delta}(OC)_{\beta+\delta}$ indicate manganese oxide in high and low oxidation states, respectively.

Manganese oxides evaluated for supercapacitor application are typically synthesized by reducing aqueous $KMnO_4$ solution with various reducing agents such as potassium borohydride, sodium dithionite, sodium hypophosphite, and hydrochloric acid under various controlled pH conditions [2]. They can also be directly deposited on metallic or graphite substrates by electrochemical anodic deposition in $Mn(CH_3COO)_2$ solution [3] or in $MnSO_4$ solution [4]. Sol–gel method has also been reported to synthesize nanostructured manganese dioxide material using manganese acetate ($MnAc_2{\cdot}4H_2O$) and citric acid ($C_6H_8O_7{\cdot}H_2O$) as the raw materials [5]. Manganese oxide was also prepared in the thin film form by anodic oxidation of metallic manganese films deposited by sputtering [6]. Electrochemical oxidation converts the sputtered Mn metal thin film into a porous, dendritic structure of manganese oxide which displays significant high specific capacitance.

Theoretical capacities of manganese oxides range from 1100 to 1300 F g^{-1} [7–11], but these high values are hardly achievable.

* Tel.: +1 519 430 7147; fax: +1 519 430 7064.
E-mail address: dongfang.yang@nrc.gc.ca

0378-7753/$ – see front matter. Crown Copyright © 2011 Published by Elsevier B.V. All rights reserved.
doi:10.1016/j.jpowsour.2011.06.045

The oxidation state of manganese ions in the oxides is a very critical factor affecting the specific capacitance. It was believed that manganese oxides involving tetravalent Mn(4+) ions such as MnO_2 exhibits much better performance than manganese oxides involving trivalent Mn(3+) and divalent Mn(2+) ions such as Mn_2O_3 and Mn_3O_4, respectively [12–14]. The pseudo-capacitive performance of manganese oxides are also affected by their microstructures and surface morphologies which are controlled by their fabrication methods and processing conditions. Since microstructures and morphology are closely related to the specific surface area, they will therefore affect the specific capacitance. Manganese oxides with amorphous or poor crystallinity structures possess porous microstructure and larger surface areas. Larger surface area implies more faradaic active sites and thereby higher pseudo-capacitance, however, the electrical conductivity for amorphous or poor crystallinity structures are relatively low. In contrast, manganese oxides with high crystallinity can give rise to higher electrical conductivity but their surface area also reduces simultaneously. Surface area reduction sometime can be compensated by the existing of tunnels in the crystalline structures such as α-, β- γ- or δ-MnO_2 for ion intercalation, therefore could provide additional pseudo-capacitance and are of great interest to be exploited [15]. Whether an amorphous or crystalline microstructure of manganese oxides is more favourable for pseudocapacitor application will depend on which factors (e.g. surface area, conductivity or tunnels) is dominant one. Most of manganese oxide prepared and used for supercapacitors has an amorphous or poor crystallinity structures and normally consists of mixed valence states in which the oxidation states of manganese ions exists in all the 2+, 3+ and 4+ (for MnO, Mn_3O_4 and Mn_2O_3), respectively. Although proper heat-treatment of amorphous manganese oxide can be used to form crystalline structure, it is normally very difficult to prepare pure phase of crystalline or amorphous manganese oxides of single valence state, therefore pseudocapacitive behaviours of various pure phase of manganese oxide with single valence state have not been well-understood [16,17]. It would be very interested to prepare manganese oxides of different phases and valence states using the same fabrication process and then compared their pseudo-capacitance behaviours in order to identify the most suitable chemical composition, phases and valence states for pseudo-capacitor applications.

As one of thin film physical vapour deposition processes, pulsed laser deposition (PLD) is very suitable for the fabrication of either amorphous or pure crystalline phase of active materials such as manganese oxides due to its flexibility and easy in controlling the deposition process parameters; therefore it possesses the great potential for supercapacitor material research. In this work, PLD process parameters will be developed in order to fabricate amorphous and pure phase of manganese oxide of different valences such as dimanganese trioxide, trimanganese tetraoxide and manganese dioxide. Si(1 0 0) wafers and polished stainless steel 316 were used as substrates for the deposition. Manganese oxide thin films deposited on Si substrates were characterized by XRD for their phase identification, while films deposited on stainless steel was evaluated by electrochemical CV for the determination of specific current and capacitance. A comparison of pseudo-capacitance of various manganese oxides with manganese at different oxidation states prepared by PLD will be given in this paper.

2. Experimental

2.1. Pulsed laser deposition (PLD) of manganese oxide thin films

Various manganese oxide films were grown on silicon and stainless steel substrates using the PLD technique. The PLD process uses a pulsed laser beam generated by a KrF excimer laser (Lambda Physik LPX-210i) operating at a wavelength of 248 nm and pulse duration of 25 ns to ablate a target and deposit thin film in an vacuum chamber (PVD products, PLD-3000). During the deposition process, the laser beam was introduced into the deposition chamber through a quartz window and focused with optical lens onto the target surface. The laser fluence on the target was adjusted to be 2–3 J cm^{-2}, while the repetition rate was fixed at 50 Hz. For the deposition of manganese oxide films, a 3.5-inch circular target of either manganese oxide (Mn_3O_4, 99.9% pure from K.J. Lesker) or metallic Mn (Mn, 99.95% pure from K.J. Lesker) was used. The laser beam ablated the rotating Mn_3O_4 or Mn target at a speed of 18 rpm in various temperatures and oxygen pressures to form manganese oxide thin films deposited directly on the 3-inch Si(1 0 0) [p-type, $\rho = 10–30\ \Omega$ cm, from Polishing Corporation of America] or 20 mm × 30 mm × 1.0 mm polished rectangular stainless steel 316 substrates. To improve the film homogeneities, the substrates were rotated along the vertical axis at a speed of 35 rpm. Before introducing a Si wafer into the deposition chamber, it was cleaned by acetone, and isopropyl alcohol, and then etched in 2.5% HF acid for 5 min to remove the native oxide. The stainless steel substrates were polished by SiC 240 micro-grits sand paper and then by Al_2O_3 paste of 0.05 μm to the mirror-like finish. They were then cleaned by acetone and isopropyl alcohol before being introduced into the deposition chamber. After loading the substrate, the system was pumped down to a base pressure below 3×10^{-7} Torr using a turbo-molecular pump. The substrate to be coated was facing the target, with a stand-off distance of 8–12 cm. During deposition, some substrates were heated, under vacuum, using a programmable non-contact radioactive heater. Oxygen gas (UHP) pressure was adjusted to be 0–500 mTorr during deposition. Detailed information about the deposition processes has been given in Ref. [18]. The film structure was examined by using X-ray diffraction equipment (XRD, Philips, X-Pert MRD) with monochromatized Cu Kα in the θ_0–2θ thin film configuration, where θ_0 was fixed at 0.5° for MnO_x films. Their surface morphology was then analyzed by a Leo 440 field emission scanning electron microscope (FE-SEM). The reflectance of the films at the ultra-violet (UV) and visible wavelength ranges was also measured using a photospectrometer from Scientific Computing International. The thickness of films determined from the reflectance data was in the range of 100–400 nm. The weight of un-coated and MnO_x films coated substrates were measured by a highly sensitive balance with precision down to 10 μg and used to calculate the weight of the MnO_x films.

2.2. Electrochemical characterization

Electrochemical characterization of manganese oxide films was performed by cyclic voltammetry (CV) in a standard three-electrode cell with 0.1 M Na_2SO_4 aqueous solution as the electrolyte. The counter electrode was a platinised platinum wire and the reference electrode was an Ag/AgCl electrode fitted with a salt bridge. The potential was cycled with a Gamry PC3 potentiostat within a potential range −0.1 to 0.9 V vs. Ag/AgCl at a scan rate of 1, 5, 10, 20 and 50 mV s^{-1}, respectively. This potential range was chosen to ensure that redox processes on manganese oxide films occur homogenously and reversibly. The test cell configuration was designed such that all the thin-film samples under testing have the same surface area (~4.6 cm^2) exposed to the electrolyte during electrochemical cycling experiments. This ensures that capacitance of MnO_x of different oxidation states and phases can be compared. The specific current and capacitance of manganese oxide films were calculated from cyclic voltammogram data and the weight of manganese oxide films. The weight of the manganese oxide films were determined by subtracting the weight of manganese oxide film coated stainless steel substrate by the bare stainless steel sub-

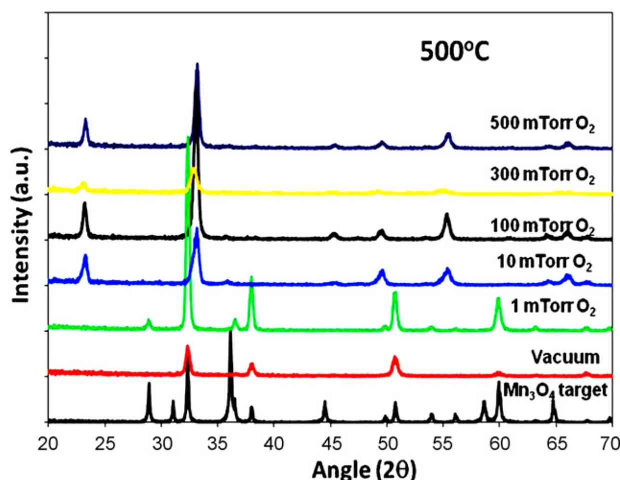

Fig. 1. XRD spectra of manganese oxide films deposited by PLD at substrate temperatures of 500 °C in various oxygen gas pressures using a Mn_3O_4 target. XRD spectrum of the Mn_3O_4 target was also shown for comparison.

strate. The electrical current and capacitance data were divided by the weight of the film to obtain the specific current and specific capacitance. Galvanostatic charge/discharge cycles of manganese oxide films of various phases were carried out at various constant currents ranging from 100 to 400 μA.

3. Results and discussion

3.1. XRD characterization of manganese oxide films deposited by PLD

XRD patterns of manganese oxide films deposited by PLD on silicon substrate using a Mn_3O_4 target at various substrate temperatures and oxygen processing gas pressures are shown in Figs. 1 and 2. XRD pattern of the Mn_3O_4 target was also presented in the figures for comparison. XRD pattern of Mn_3O_4 target can be identified as the tetragonal structure (PDF card #24-0734) [19]. Excimer laser ablation of Mn_3O_4 target at substrate temperature of 500 °C in vacuum and oxygen pressure lower than 1 mTorr produced also a pure tetragonal Mn_3O_4 phase (PDF card #24-0734), however, some diffraction peaks shown in Mn_3O_4 target such as peaks at 2θ = 31.0, 36.1, 58.5, 64.7 which correspond to diffraction from index planes of (2 0 0), (2 1 1), (3 2 1) and (4 0 0), respectively, disappeared. This suggested Mn_3O_4 film deposited on Si(1 0 0) has preferential orientation. When oxygen pressure during the PLD process increased to values higher than 10 mTorr, a pure Mn_2O_3 phase was formed. XRD patterns of Mn_2O_3 films can be identified as either a cubic structure (PDF card #41-1442) or an orthorhombic structure (PDF card #24-0508). Due to similarity in the XRD patterns of both structures, it is hard to judge whether a cubic or an orthorhombic structure was formed. The XRD peaks for the Mn_2O_3 film deposited at 300 vmTorr O_2 are weaker than those of peaks for the Mn_2O_3 films deposited at 500 vmTorr and 100 mTorr O_2, respectively. This is due to the thickness of this particular film is thinner than the other two. Fig. 2(a) shows XRD patterns of manganese oxide films deposited at the substrate temperature of 200 °C in oxygen pressure ranging from 1 mTorr to 500 mTorr. At 1 mTorr oxygen pressure, the pure crystalline Mn_3O_4 phase was deposited, while at oxygen pressure higher than 100 mTorr an amorphous phase was formed as shown in the figure. Fig. 2(b) gives XRD patterns of manganese oxide films deposited in 250 mTorr O_2 pressure at substrate temperatures ranging from 400 °C to 500 °C. Amorphous MnO_x films were produced at substrate temperatures below 450 °C, while at 500 °C the pure crystalline Mn_2O_3 phase was

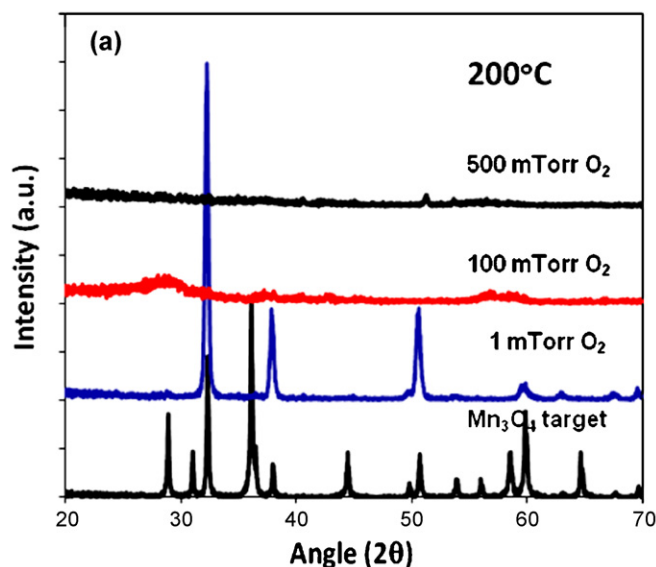

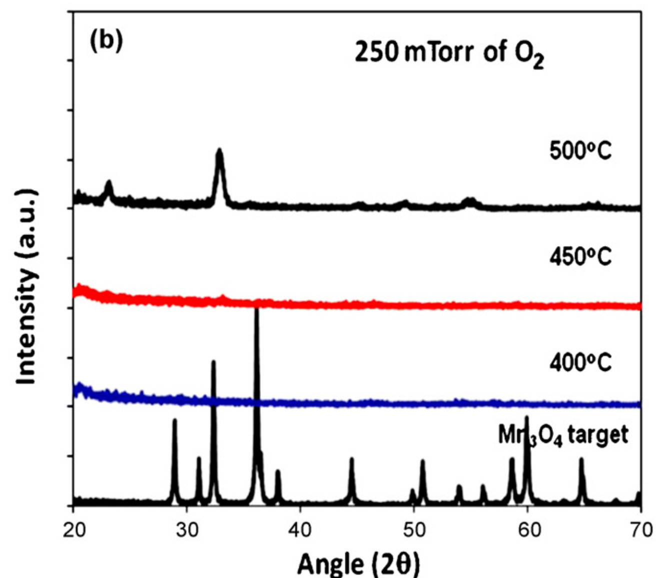

Fig. 2. XRD spectra of manganese oxide films deposited by PLD at (a) 200 °C in various oxygen gas pressures and in (b) 250 mTorr of oxygen pressure at various temperatures using a Mn_3O_4 target. XRD spectrum of the Mn_3O_4 target was also shown for comparison.

formed. The oxidation state of Mn (either +2, +3 or +4) in amorphous films, unfortunately, cannot be determined basing on XRD patterns.

XRD patterns of manganese oxide films deposited by PLD on silicon substrate using a metallic Mn target at various substrate temperatures and oxygen pressures are shown in Figs. 3 and 4. XRD pattern of the Mn target was also presented in the figures for comparison. The XRD pattern of Mn target can be identified as the cubic structure α-Mn (PDF card #32-0637). At 700 °C substrate temperature, laser ablation of the Mn target in oxygen pressure of 1 mTorr produced the pure tetragonal Mn_3O_4 phase (PDF card #24-0734), similar to the film deposited in the same oxygen pressure at 500 °C using the Mn_3O_4 target. When the oxygen pressure increased to 10 mTorr of O_2, mixed phases of Mn_3O_4 and Mn_2O_3 co-formed in the film. When oxygen pressures are higher than 20 mTorr, only the pure crystalline Mn_2O_3 phase appeared in the deposited films. When manganese oxide films deposited at temperatures of 400 °C or lower in 40 mTorr O_2 as shown in Fig. 4(a), they consist of amorphous manganese oxides MnO_x and cubic structure

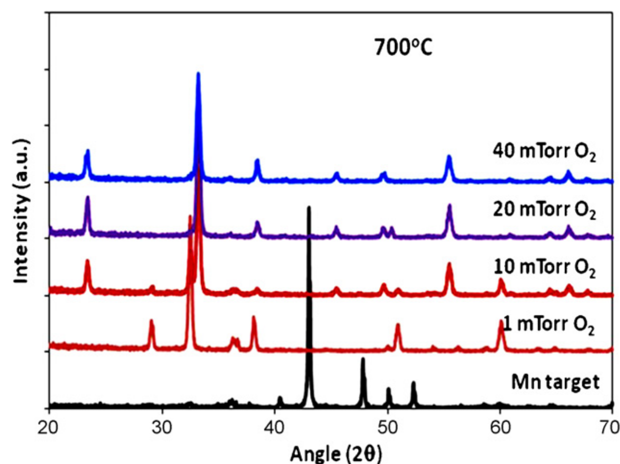

Fig. 3. XRD spectra of manganese oxide films deposited by PLD at substrate temperatures of 700 °C in various oxygen gas pressures using a Mn target. XRD spectrum of the Mn target was also shown for comparison.

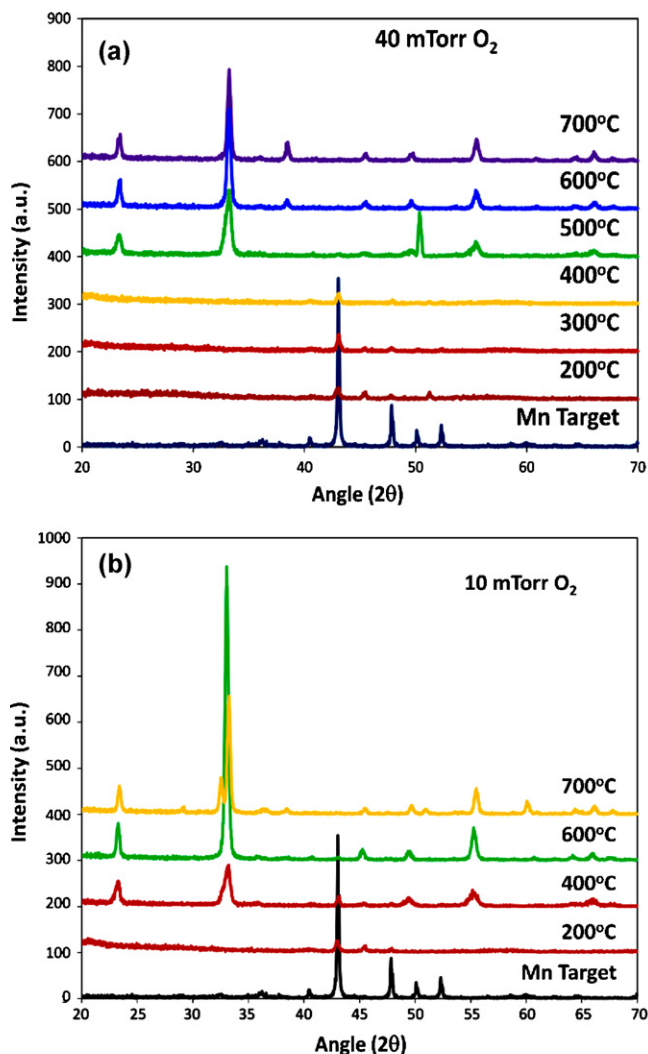

Fig. 4. XRD spectra of manganese oxide films deposited by PLD at (a) 40 mTorr and (b) 10 mTorr of O_2 pressure at various substrate temperatures using a Mn target. XRD spectrum of the Mn target was also shown for comparison.

α-phase metallic Mn (and possibly some β-Mn as indicating by diffraction peaks at $2\theta = 45$), which indicate that under low substrate temperatures, not all the metallic Mn vapour (plume) was oxidized to form manganese oxides, therefore metallic α-phase still existed in the films. In the same 40 mTorr O_2, laser ablation of Mn target at 500 °C or higher produced only pure crystalline Mn_2O_3 phase indicating that all the Mn vapour was totally oxidized to form the oxide. It is also very interested to see that in lower O_2 pressure of 10 mTorr, even at a temperature as low as 400 °C, Mn_2O_3 phase can be deposited as shown in Fig. 4(b). Only when the substrate temperature reaches over 700 °C, films consisting of mixed Mn_3O_4 and Mn_2O_3 phases were deposited. XRD results in Figs. 1–4 clearly demonstrate that by controlling the processing parameters of the PLD technique, a pure phase of either crystalline Mn_2O_3 or Mn_3O_4, a mixed phase of crystalline Mn_2O_3 and Mn_3O_4, a mixed phase of metallic Mn and amorphous MnO_x, as well as an amorphous phase MnO_x can be successfully prepared. The microstructures of manganese oxide films deposited by PLD at various temperatures and oxygen pressures were very different as revealed by FE-SEM. Fig. 5 shows typical examples of the FE-SEM topography images of manganese oxide films deposited on Si(1 0 0) substrates. The grain size, surface roughness and grain orientation of manganese oxide films deposited at 200 °C in 100 mTorr O_2, 500 °C in 1 mTorr O_2, and 500 °C in 100 mTorr O_2, respectively, are very much dependent on the temperature and oxygen pressure during the PLD process as shown in the figure. This is consistent with the XRD results in Figs. 1–4. The ability of the PLD technique to produce manganese oxides with different oxidation states, phases and microstructures allows us to identify the best structures and compositions of active material candidates for supercapacitor applications. Unfortunately, neither a pure phase MnO_2 or MnO can be obtained by PLD using a Mn_3O_4 or a metallic Mn target within our system's temperature range of 20–750 °C and oxygen pressure range of 2×10^{-7}–500 mTorr. According to the oxygen pressure–temperature phase diagram of manganese oxide described in Fig. 2 of Ref. [20], the conditions for thermodynamically stable MnO phase to exist in the temperature range of 20–750 °C, the oxygen partial pressure has to be lower than 10^{-11} atmosphere which is unachievable in the PLD system used in this study. Although PLD is well-known for the ability to deposit thermodynamically unstable phase due to the non-equilibrium nature of the technique, it is unlikely that MnO phase can be deposited since the temperature and pressure values are too far away from their equilibrium conditions. Although the resulting phases of manganese oxides prepared in our PLD experiments using either Mn_3O_4 or Mn target did not exactly match what are predicted by the phase diagram, the conditions at which individual phase was deposited are not too far away from its equilibrium conditions described in the phase diagram. According to the diagram, MnO_2 phase is thermodynamically stable at temperatures lower than 300 °C when the oxygen partial pressure is less than 1 Torr; therefore, the amorphous MnO_x films deposited at 200 °C and 100 mTorr O_2 in this work, very likely, was an amorphous MnO_2. Tabbal et al. reported [21] that laser ablation of a MnO target in oxygen gas ambient above 250 mTorr and an optimal deposition temperature of 500 °C, crystalline MnO_2 phase can be deposited on Si substrates. However, under such conditions, the thermodynamically stable phases are either pure Mn_2O_3 phase or mixed Mn_2O_3 and Mn_3O_4 phases but not the MnO_2 according to the phase diagram. An effort to reproduce those results is currently underway and the results will be reported in our future communication.

3.2. Electrochemical characterization of manganese oxide films

Fig. 6 compared the cyclic voltammograms (CV) of manganese oxide films of different phases deposited on polished stainless steel

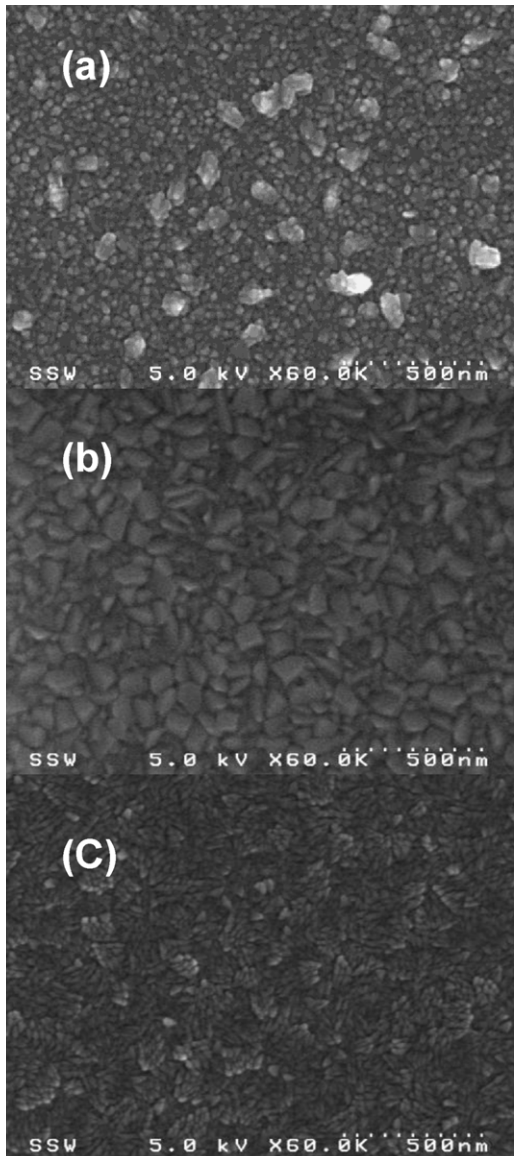

Fig. 5. FE-SEM topography images of manganese oxide films deposited by PLD on Si(1 0 0) substrates at (a) 200 °C in 100 mTorr O_2, (b) 500 °C in 1 mTorr O_2, and (c) 500 °C in 100 mTorr O_2.

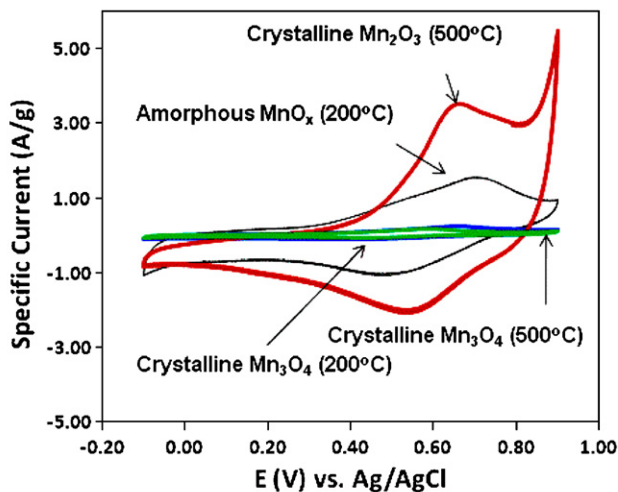

Fig. 6. Cyclic voltammograms of manganese oxide films deposited by PLD at various substrate temperatures and oxygen gas pressures.

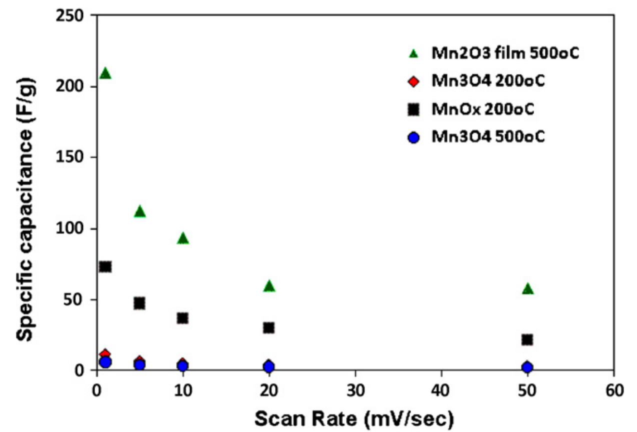

Fig. 7. Specific capacitance vs. CV scan rates for manganese oxide films deposited by PLD at various substrate temperatures and oxygen gas pressures.

316 substrates at various conditions. For comparison of different manganese oxide films, the measured electric current in CV was normalized by the weight of the films and reported as specific current vs. electric potential. It is clearly to see that crystalline Mn_3O_4 films deposited in low oxygen pressure of 1 mTorr O_2 at both 200 °C and 500 °C has the lowest specific current in the CV which indicates that Mn_3O_4 phase has the poorest pseudo-capacitance behaviours. Crystalline Mn_2O_3 phase deposited at 500 °C and 100 mTorr shows the highest specific current. The amorphous MnO_x film deposited in 100 mTorr O_2 at 200 °C has the second highest specific current. The curves of specific capacitance vs. CV scan rate of different phases of manganese oxides are shown in Fig. 7. Specific capacitance of the pure Mn_3O_4 phase at 50 mV s^{-1} scan rate is only 3 F g^{-1}, while at 1 mV s^{-1} it is 12 F g^{-1}. Crystalline Mn_2O_3 film has the highest specific capacitance. It has a specific capacitance of 58 F g^{-1} at 50 mV s^{-1} scan rate and reaches 210 F g^{-1} at 1 mV s^{-1} scan rate. The specific capacitances of the amorphous MnO_x film are 25 F g^{-1} at 50 mV s^{-1} and 77 F g^{-1} at 1 mV s^{-1}, respectively. The specific capacitance increases with the decrease in scan rate for all the manganese oxide film indicates that kinetic of surface redox reactions of manganese oxide is relatively slow and the charging–discharging process of manganese oxide films does not behave like an ideal double layer capacitor. It could also indicate that resistance existed for ions of electrolyte to diffuse into the PLD manganese oxide films. Fig. 8 gives the Galvanostatic charge/discharge cycles of manganese oxide films of different phases at constant currents ranging from 100 to 400 μA (or 22 to 87 μA cm^{-2}). The specific capacitance, calculated from charge/discharge curves, for crystalline Mn_3O_4 phase

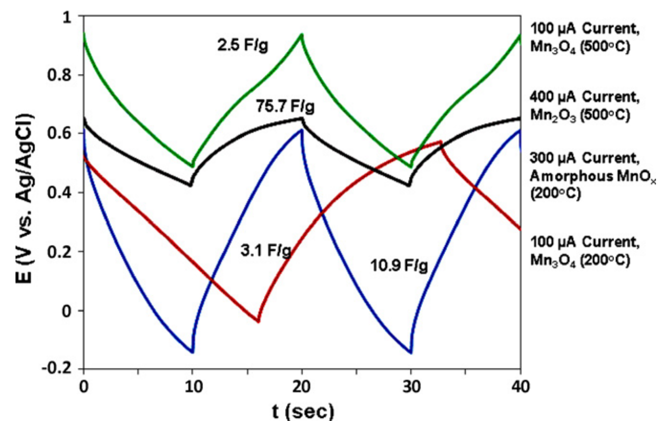

Fig. 8. Galvanostatic charge/discharge cycles of various manganese oxide films in 0.1 M K_2SO_4 at various constant currents.

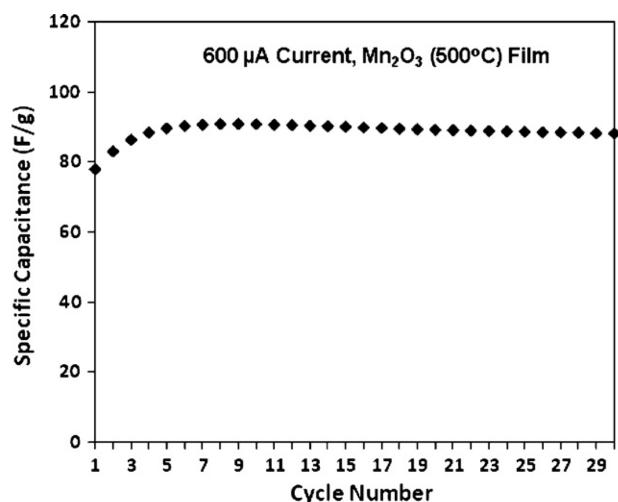

Fig. 9. The Galvanostatic charge/discharge cycling behaviour of the crystalline Mn_2O_3 film at constant currents of 600 μA (131 μA cm^{-2}).

deposited at 500 °C and 200 °C are 2.5 F g^{-1} and 3.1 F g^{-1}, respectively. The crystalline Mn_2O_3 phase has the specific capacitance of 75.5 F g^{-1} and the amorphous MnO_x was 10.9 F g^{-1}. Again the crystalline Mn_2O_3 film gives highest specific capacitance value and is consistent with the data obtained from CVs. The Galvanostatic charge/discharge cycling behaviour of the crystalline Mn_2O_3 film at constant current of 600 μA (131 μA cm^{-2}) was also studied and the results are shown in Fig. 9. The specific capacitance of the crystalline Mn_2O_3 film, calculated from discharge curves, increases from original value of 78 F g^{-1} to around 91 F g^{-1} after 8 cycles which could be attributed to the increase of surface roughness due to cycling, and then becomes almost constant throughout the rest 30 cycles. The degradation in specific capacitance from cycles 8 (91 F g^{-1}) to cycle 30 (88 F g^{-1}) is less than 3.3%. Since the cycling data presented in Fig. 9 is for a very thin Mn_2O_3 film (around 120 nm), it normally should degrade much more than the conventional supercapacitor electrode where much thicker active materials (>100 μm) is used. As the pseudo-capacitance behaviour is only originated from surface/subsurface redox reactions, thicker film of active materials is expected to degrade more slowly as long as the material is stable and attached well to the current collector. The very slow degradation of such thin Mn_2O_3 film indicated that the stability and cyclic durability of the crystalline Mn_2O_3 film is excellent.

Most of the literature reports suggested that MnO_2 exhibits better pseudo-capacitance performance than that of $Mn(OH)_2$, Mn_2O_3, and Mn_3O_4 [7–9], in this study, however, crystalline Mn_2O_3 films was found to be better than amorphous MnO_x films (which very likely is an amorphous MnO_2 according to the phase diagram). The better performance of the crystalline Mn_2O_3 film than the amorphous MnO_2 film may due to relatively higher electrical conductivity and better electrical contact with the current collector of a crystalline phase than an amorphous phase. Crystalline MnO_2 film, unfortunately, was unable to be fabricated in this study, and hence a comparison between the specific capacitances of the crystalline MnO_2 and Mn_2O_3 films cannot be given. The crystalline manganese oxide films such as Mn_2O_3 and Mn_3O_4 prepared by PLD in this study are pure and have very well-defined crystal structures and surface morphologies as indicating by XRD. Such pure crystalline phases are hard to be prepared by wet-chemical or electrochemical methods and could provide really reliable pseudo-capacitance data for comparison of manganese oxides of difference phases and valence states. In this study, not all the phases and valance states of manganese oxides have been successfully prepared; therefore a completed comparison of all materials cannot be given. The pseudo-capacitance data that were obtained in this study also consist with results reported by some other researchers. For example, relatively high specific capacitance (∼100 F g^{-1} at 5 mV s^{-1}, very close to this study) of Mn_2O_3 nanospheres was also reported by Nathan et al. in alkaline medium [22]. The authors believed that Mn_2O_3 samples exhibit simple redox reaction via Mn^{3+}/Mn^{4+} couple yielding one electron transfer and they attributed the high pseudocapacitance to the presence of facile crystal structure that facilitates the easy insertion/removal of electrolyte ions (OH^-) in Mn_2O_3 nanospheres. Very low specific capacitance value was also observed by Dubal et al. [23] for Mn_3O_4 thin films prepared by a chemical bath deposition method, however, they found that the interlocked cubelike Mn_3O_4 film can be transformed to nanoflakes of layered birnessite MnO_2 using voltammetric cycling in 1 M Na_2SO_4 electrolyte at 100 mV s^{-1} scan rate within the potential window of 0.1 to +0.9 V. The specific capacitance of Mn_3O_4 films increased from 11.8 to 139.3 F g^{-1} at 100 mV s^{-1} after 3000 potential cycles. In an acid medium (e.g. HCl), however, an irreversible dissolution of Mn_3O_4 could take place during the potential scan [24]. Actually, Mn_3O_4 films deposited by PLD in this study were found to delaminate from stainless steel substrate after long time potential cycles which did not occurred for crystalline Mn_2O_3 and amorphous MnO_x films. The specific current and capacitance of all the manganese oxide films increased after long time cycling between potential −0.1 and 0.9 V vs. Ag/AgCl, The crystalline Mn_2O_3 films increased the most and its specific capacitance reached 108 F g^{-1} at 50 mV s^{-1}. After long time cycling, it was also interested to find that the increase in specific capacitance at high scan rate is much larger than at low scan rate and different in specific capacitance at various scan rate was decreased. The reason for the increase in specific capacitance by cycling is believed to be due to the increase in the surface roughness and porosity of the PLD manganese oxide films after cycling. More rough and porous film will reduce the resistance for ions to move in/out of the manganese oxide film, therefore increase the specific capacitance at high scan rates. In the case of Mn_3O_4, the increase in capacitance could also due to transformation of Mn_3O_4 to MnO_2 as reported in Ref. [23].

4. Conclusion

PLD technique has been used in this study to deposit the manganese oxide film on Si(1 0 0) and stainless steel substrates. By varying the deposition processing parameter conditions such as substrate temperature and oxygen pressure, pure phases of crystalline Mn_2O_3, Mn_3O_4 as well as an amorphous phase of MnO_x were successfully grown. The specific current and capacitance of different manganese oxide films determined by cyclic voltammetry show that polycrystalline Mn_2O_3 phase has the highest specific current and capacitance, while the values for polycrystalline Mn_3O_4 films are the lowest. The specific current and capacitance values of the amorphous MnO_x film are lower than crystalline Mn_2O_3 but higher than crystalline Mn_3O_4 film. The specific capacitance of Mn_2O_3 film reaches 200 F g^{-1} at 1 mV s^{-1} scan with excellent stability and cyclic durability. This work demonstrated that PLD is a very promising technique for supercapacitor material research due to its excellent flexibility and capability of controlling microstructures and phases of various materials.

Acknowledgements

The authors would like to thank Transport Canada and National Research Council of Canada's automotive office for supporting this supercapacitors project. The author is also indebted to Mr. B. Gibson and Mr. M. Zeman of NRC-IMI for their technical assistance.

References

[1] P. Simon, Y. Gogotsi, Nat. Mater. 7 (11) (2008) 845–854.
[2] Y.U. Jeong, A. Manthiram, J. Electrochem. Soc. 149 (11) (2002) A1419–A1422.
[3] Q. Huang, X. Wang, Electrochim. Acta 52 (4) (2006) 1758–1762.
[4] K.R. Prasad, N. Miura, J. Power Sources 135 (1–2) (2004) 354–360.
[5] X. Wang, A. Yuan, J. Power Sources 172 (2) (2007) 1007–1011.
[6] J.N. Broughton, M.J. Brett, Electrochim. Acta 49 (25) (2004) 4439–4446.
[7] S. Shiraishi, M. Kibe, T. Yokoyama, H. Kurihara, N. Patel, A. Oya, Y. Kaburagi, Y. Hishiyama, Appl. Phys. A 82 (2006) 585.
[8] D.-W. Wang, F. Li, Z.-G. Chen, G.Q. Lu, H.-M. Cheng, Chem. Mater. 20 (2008) 7195.
[9] M. Hughes, M.S.P. Shaffer, A.C. Renouf, C. Singh, G.Z. Chen, D.J. Fray, A.H. Windle, Adv. Mater. 14 (2002) 382.
[10] M. Hughes, G.Z. Chen, M.S.P. Shaffer, D.J. Fray, A.H. Windle, Chem. Mater. 14 (2002) 1610.
[11] Girish Arabale, Deepali Wagh, Kulkarni Mahesh, I.S. Mulla, S.P. Vernekar, K. Vijayamohanan, A.M. Rao, Chem. Phys. Lett. 376 (2003) 207.
[12] S.C. Pang, M.A. Anderson, T.W. Chapman, J. Electrochem. Soc. 147 (2000) 444.
[13] C.C. Hu, T.W. Tsou, Electrochem. Commun. 4 (2002) 105.
[14] R.H. Ma, Y. Bando, L.Q. Zhang, T. Sasaki, Adv. Mater. 16 (2004) 918.
[15] T. Brousse, M. Toupin, J. Electrochem. Soc. 153 (12) (2006) A2171–A2180.
[16] J.K. Chang, Y.L. Chen, J. Power Sources 135 (1–2) (2004) 344–353.
[17] J.K. Chang, W.T. Tsai, J. Electrochem. Soc. 152 (10) (2005) A2063–A2068.
[18] S. Boughaba, G.I. Sproule, J.P. McCaffrey, M. Islam, M.J. Graham, Thin Solid Films 358 (2000) 104–113.
[19] Joint Committee on Powder Diffraction Standards, International Center for Diffraction Data, 1996.
[20] D. Kwon, T. Akiyoshi, H. Lee, M.T. Lanaganz, J. Am. Ceram. Soc. 91 (3) (2008) 906–909.
[21] M. Tabbal, M. Abi-Akl, S. Isber, E. Majdalani, T. Christidis, Proc. SPIE Vol. 7201 720104-1-6.
[22] T. Nathan, M. Cloke, S.R.S. Prabaharan, J. Nanomater. 2008 (2008) 8 (article ID 948183).
[23] Deepak P. Dubal, Dattatray S. Dhawale, Rahul R. Salunkhe, Chandrakant D. Lokhande, J. Electrochem. Soc. 157 (7) (2010) A812–A817.
[24] Vadim B. Fetisov, Galina A. Kozhina, Alexander N. Ermakov, Andrey V. Fetisov, Elena G. Miroshnikova, J. Solid State Electrochem. 11 (2007) 1205–1210.